







Cite this: *Phys. Chem. Chem. Phys.*,
2019, 21, 25047

Electrochemical CO₂ reduction on Cu and Au electrodes studied using *in situ* sum frequency generation spectroscopy†

Zhi-Chao Huang-fu,  Qian-Tong Song, Yu-Han He, Jing-Jing Wang, Jin-Yu Ye, Zhi-You Zhou,  Shi-Gang Sun * and Zhao-Hui Wang *

As an important pathway for energy storage and a key reaction in the carbon cycle, the CO₂ electrochemical reduction reaction has recently gained significant interest. A variety of catalysts have been used to approach this topic experimentally and theoretically; however, the molecular level insight into the reaction mechanism is lacking due to the complexity of the surface processes and the challenges in probing the intermediate species. In this study, CO₂ reduction reactions on polycrystalline Cu and Au electrodes were investigated in 0.1 M CO₂-saturated NaHCO₃ solution. *In situ* sum frequency generation (SFG) spectroscopy has been adopted to access the intermediates and products on the metal electrodes. On the Au electrode, only linearly adsorbed CO could be detected, and the reduction produced no hydrocarbon species. On the Cu electrode, C–H stretching vibrations corresponding to surface-adsorbed ethoxy species were observed, but no CO vibrations can be detected with SFG. The results revealed that the CO randomly adsorbed on the Cu surface, and the multiple orientations of the adsorbed species may be the reason for the formation of C–C bonding. These results demonstrate direct molecular level evidence for different reaction pathways on the Cu and Au electrodes.

Received 5th August 2019,
Accepted 14th October 2019

DOI: 10.1039/c9cp04346b

rsc.li/pccp

Introduction

The electrocatalytic reduction of carbon dioxide has attracted the interest of electrochemists for decades as it can accomplish the conversion of CO₂ to valuable carbon resources.^{1–3} The application of electrochemical reduction of CO₂ to hydrocarbons is promising and challenging. The major problems hindering the utilization of electrochemical CO₂ reduction are the high overpotentials needed and the poor product selectivity and low faradaic efficiency.^{4–7} To improve the selectivity and efficiency, insightful understanding of the mechanisms should be obtained through experimental and theoretical investigations of CO₂ reduction on a variety of catalysts.

Metal^{8–17} and molecular/organic catalysts^{18–20} have been adopted for CO₂ reduction to accomplish the transformation of CO₂ to other valuable products. In 1985, Hori *et al.* discovered that Cu can electrochemically reduce CO₂ to different hydrocarbons, such as methane, ethylene, and ethanol, with fairly high faradaic efficiency.²¹ On the other hand, other metals will

only produce relatively simple reduced species. For example, Au and Ag produce CO primarily, and other post-transition-metals, such as indium and lead, can convert CO₂ into formate. Compared to C1 products (CO, methane, and methanol), C2 and long-chain hydrocarbons (ethylene, ethanol, propanol, *etc.*) have a higher market price and a wider application prospect.²² Substantial effort has been invested to understand the role of Cu in the CO₂ reduction reaction.^{7,21,23–38} However, more than 10 different hydrocarbon products could be simultaneously detected in the CO₂ reduction on Cu.^{29,39} The poor selectivity limited the further application of Cu. To form C2 products, kinetic and energetic barriers have to be overcome on the electrode surfaces. Multiple step reaction pathways of CO₂ reduction on Cu, typically starting with the formation of adsorbed CO (*CO) species, have been proposed based on density functional theory (DFT) simulations and experimental findings.^{4,23,40,41} The reaction precursor and key intermediate, *CO, along with some other reaction intermediates involved in the CO₂ reduction, has been investigated with *in situ* spectroscopy.^{5,6,9,28,42–49} The formation of the C–C bond *via* direct dimerization of *CO on the Cu electrode surface was supported by the observation of C–O–H and C=O stretching modes of a hydrogenated dimer intermediate (OCCOH) with *in situ* infrared (IR) spectroscopy.⁶ Surface enhanced infrared absorption spectroscopy (SEIRAS) in an attenuated total reflection (ATR)

Collaborative Innovation Center of Chemistry for Energy Materials, State Key Laboratory for Physical Chemistry of Solid Surface, Department of Chemistry, College of Chemistry and Chemical Engineering, Xiamen University, Xiamen 361005, China. E-mail: sgsun@xmu.edu.cn, zhwang@xmu.edu.cn

† Electronic supplementary information (ESI) available. See DOI: 10.1039/c9cp04346b

configuration is free from bulk layer absorption, high solution resistance, and inhomogeneous current distribution in probing adsorbed species on electrodes. The formation and behavior of *CO were observed and studied by ATR-SEIRAS on Cu films, and possible intermediates in the low frequency range were detected.^{48,49} The influence of water in the CO₂ reduction at the Cu electrode in acetonitrile solutions was investigated by Koper *et al.* with surface enhanced Raman spectroscopy (SERS).⁵ Unfortunately, the low molecular density and weak adsorption made it very difficult to thoroughly investigate the hydrocarbon intermediates on the electrode surface. In particular, sum frequency generation (SFG) spectroscopy, with its intrinsic surface/interface selectivity, has been used to characterize the CO₂ reduction processes in room-temperature ionic liquids (RTIL)^{50–52} and with Re/Mn heterogenized molecular catalysts.^{15,53–56} However, most studies of the SFG spectroscopy of CO₂ reduction still focused on the detection of *CO; so far, there is still a lack of molecular level information in the C–H stretching vibrational region. In order to draw a full roadmap of the reaction pathways and reveal the mechanism of the CO₂ reduction on Cu, detailed spectroscopy of the primary steps of CO₂ reduction and C2 formation should be carried out.

In this study, we used broadband SFG (BB-SFG) spectroscopy to investigate the CO₂ electrochemical reduction processes on polycrystalline Cu and Au electrodes in 0.1 M CO₂-saturated NaHCO₃ solution. The BB-SFG spectra covering both the C–H and C–O stretching vibrations and the spectral evolution with surface potentials on Cu, Au and Cu sub-monolayer modified Au electrodes were analyzed. On the Cu electrode, the formation of C2 species was identified, and CO was the main product on the Au electrode.

Experimental section

Laser and SFG setup

The BB-SFG spectroelectrochemistry apparatus has been described elsewhere;^{57–59} details can be found in the ESI.† Briefly, the output of a femtosecond Ti:sapphire laser (Coherent Inc., Legend Elite Duo) was used to pump 2 optical parametric amplifiers (Light Conversion) to generate tunable broadband infrared pulses (IR, 2.6–10 μm, 150 fs, and 160 cm⁻¹ FWHM) and narrow-band visible pulses (VIS, 470–900 nm, 2.5 ps, and 7 cm⁻¹ FWHM). For different surface species, IR was set to 2900 cm⁻¹ (C–H species) and 2050 cm⁻¹ (*CO), respectively. The VIS (5 μJ) and IR (8 μJ) were overlapped on the electrode surface with approximately 60° incident angles. All the BB-SFG spectra were acquired with the *ppp* polarization combination, and recorded by a spectrograph (Andor Technology, SR-303i-B) with a CCD detector (Andor Technology, DU920P-BR-DD). The surface potential was controlled by a CHI604D potentiostat for the *in situ* measurements.

Principle of SFG

Details of the SFG principle have been thoroughly discussed elsewhere.^{60–65}

In BB-SFG, a picosecond visible light ω_{VIS} and a femtosecond infrared light ω_{IR} are used to generate the SFG signal at $\omega_{\text{SFG}} = \omega_{\text{VIS}} + \omega_{\text{IR}}$. The intensity of the SFG signal, $I_{\text{SFG}}(\omega)$, is given by

$$I_{\text{SFG}} \propto |P_{\text{SFG}}(\omega)|^2 = |\chi^{(2)} E_{\text{IR}} E_{\text{VIS}}|^2 \quad (1)$$

where P_{SFG} is the induced polarization. $\chi^{(2)}$, the second order susceptibility, can be separated into contributions of the infrared-frequency dependent resonances of the adsorbates and contribution of the interfacial electrons that are insensitive to the IR frequency (mainly from the electrode surfaces in this work):

$$\chi^{(2)} = \chi_{\text{NR}}^{(2)} + \chi_{\text{R}}^{(2)} = A_{\text{NR}} e^{i\theta} + \sum_q \frac{A_q}{\omega_{\text{IR}} - \omega_q + i\Gamma_q} \quad (2)$$

where A_{NR} is the oscillation strength of the nonresonant, θ is the phase difference between the resonant and nonresonant, and A_q , ω_q and Γ_q are the oscillation strength, frequency and half width of the q th mode vibrations of the resonances.

Spectroelectrochemical measurements

Spectroelectrochemical SFG experiments were carried out in the electrochemical cell as illustrated in Fig. 1, which was used previously.⁵⁷ The glass body of the cell was sealed with a CaF₂ window (∅ 32 mm with 1 mm thickness) and fixed on a stainless-steel base plate. The working electrodes were Cu and Au polycrystalline ∅ 6 mm cylinders, which were embedded in PTFE holders with metal surfaces exposed to the electrolytes. The electrode was pressed against the CaF₂ window to form a thin electrolyte layer during measurements. A flame-annealed platinum sheet (99.99%) and a commercial saturated calomel electrode (SCE) electrode served as the counter and reference electrodes, respectively. During the CO₂ reduction process, CO₂ was bubbled into the cell to maintain saturation. To investigate surface species at different potentials, chronoamperometry was carried out in the potential window of interest during the SFG measurements.

Results and discussion

Electrochemical characterization of the metal electrodes

Three metal electrodes were used in the CO₂ reduction experiments: Cu, Au, and underpotential deposition (UPD) Cu on Au

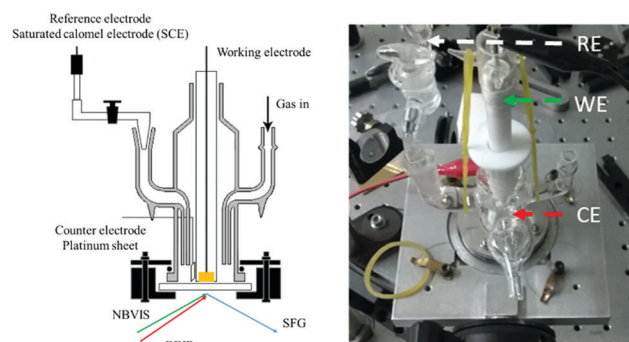


Fig. 1 Schematic of the *in situ* SFG cell.

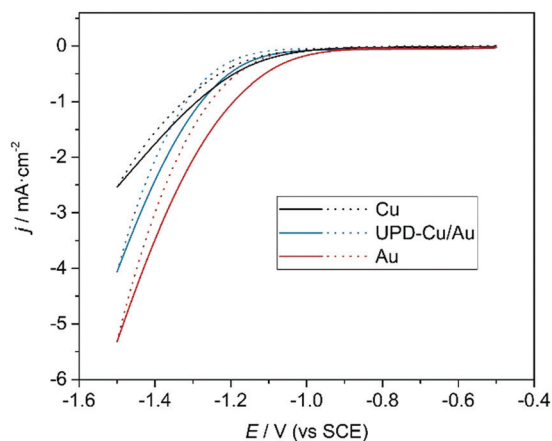


Fig. 2 Cyclic voltammograms for different electrodes (black for Cu, blue for UPD-Cu/Au, and red for Au) in 0.1 M CO₂-saturated NaHCO₃ solution (E vs. SCE); negative scan (solid lines) and positive scan (dashed lines).

(UPD-Cu/Au). Fig. 2 shows the cyclic voltammograms (CVs) for the three electrodes in 0.1 M CO₂-saturated NaHCO₃ solution (pH 6.8). With potential scanning negatively, the reductive current starts to increase around -0.9 to -1.0 V, where 2 competitive reactions, the CO₂ reduction and hydrogen evolution reaction (HER), initiate. The Au electrode showed a larger reaction current and an earlier threshold potential than that of the Cu electrode, and the CV curve of UPD-Cu/Au appeared in-between that of the Cu and Au electrodes. Except for the threshold potential and reaction current, the shapes of the CVs for the three electrodes were quite similar. Additionally, the CO₂ reduction and HER simultaneously initiated at the threshold potentials. The roles of Cu and Au in the CO₂ reduction could not be identified from the CV measurements. *In situ* spectroscopy should be carried out to reveal the reaction mechanisms with molecular level information.

BB-SFG spectra of *CO

In the CO₂ reduction reaction, it is known that ethylene, methane, ethanol and other hydrocarbons are formed at the Cu electrode through different reaction mechanisms; however, *CO is a key intermediate in the primary steps in most of the proposed reaction pathways.^{5,7,16,25,33,36} The BB-SFG observation range was set to 1950–2200 cm⁻¹ by tuning the IR to 4800 nm to cover the possible stretching vibrations of the carbon–oxygen double bonds. Fig. 3 displays the BB-SFG spectra on Au, Cu and UPD-Cu/Au electrodes. On the Au electrode, a resonant SFG band around 2100 cm⁻¹, which redshifts with the surface potential, could be observed. However, on Cu, no resonant SFG bands could be seen. For the UPD-Cu/Au electrode, the 2100 cm⁻¹ resonant SFG band with relatively weaker intensity than that of the Au electrode was detected.

To better understand the resonant SFG band, we obtained the resonant SFG spectra by fitting the BB-SFG spectra with eqn (3), and the results are displayed in Fig. 4 (details in the ESI†). As shown in Fig. 4(c) and (d), black for Au and red for UPD-Cu/Au, the intensity and band position of the 2100 cm⁻¹

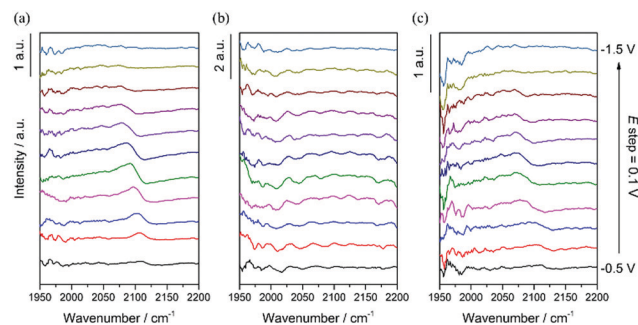


Fig. 3 Potential-dependent BB-SFG spectra (C–O region) of CO₂ reduction in 0.1 M CO₂-saturated NaHCO₃ solution on (a) Au, (b) Cu, and (c) UPD-Cu/Au electrodes (normalized with the broadband nonresonant). Offset for comparison.

resonant SFG band evolved with electrode potential almost identically. The Stark slopes at -0.5 to -1.3 V were measured as 44.4 cm⁻¹ V⁻¹ and 46.4 cm⁻¹ V⁻¹ on Au and UPD-Cu/Au electrodes, respectively. In previous IR studies, the 2100 cm⁻¹ IR absorption was assigned to the linearly bonded CO (CO_L) absorption band on Au surfaces.^{66–71} Thus, the observed SFG band may be assigned to CO_L on the Au surface as well.

$$I_{\text{SFG}} = \left| \left(A_{\text{NR}} + \sum_j \frac{A_{\text{R}} e^{i\theta_j}}{\omega_{\text{IR}} - \omega_j + i\Gamma_j} \right) \exp \left(- \left(\frac{\omega_{\text{IR}} - \omega_0}{\sigma} \right)^2 \right) \right|^2 \quad (3)$$

To further prove this assignment, BB-SFG spectral evolution with electrode potential was investigated with CO directly bubbled onto the Cu and Au electrodes. The electrode was placed in a CO-saturated 0.1 M NaClO₄ solution for 10 min to

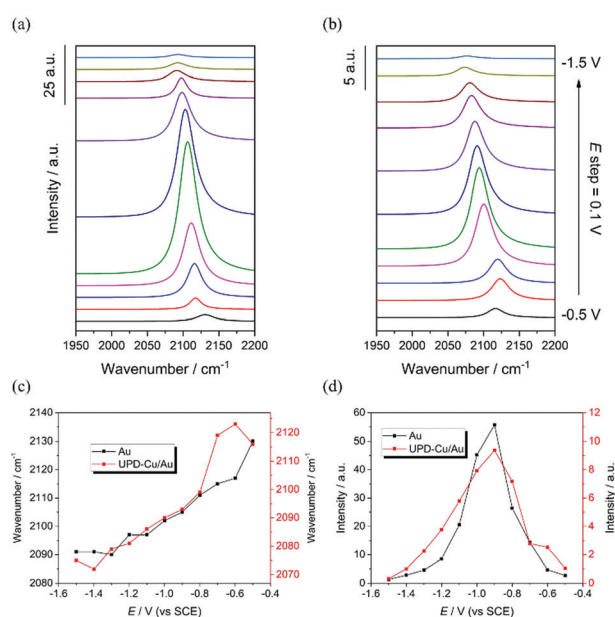


Fig. 4 Potential-dependent BB-SFG spectra of 0.1 M CO₂-saturated NaHCO₃ solution at (a) Au electrode and (b) UPD-Cu on poly-Au electrode. Potential-dependent (c) band positions and (d) intensities of the two electrodes from the fitting results (black for Au, and red for UPD-Cu/Au).

ensure formation of a CO adsorbate layer on the metal surface. Electrode potential was scanned from -0.3 V down to -1.5 V, which was similar to that for the CO_2 reduction experiments. Fig. 5 shows the BB-SFG spectra and resonant spectra for the Au electrode. The observed SFG band at ~ 2100 cm^{-1} is quite similar to that in Fig. 3(a) for CO_2 reduction on the Au electrode. The difference with Fig. 3(a) consists of the fact that the CO_L SFG band appeared at a relatively high potential ~ -0.3 V and reached the maximum at ~ -0.7 V instead of -1.1 V, as shown in Fig. 5(c). The CO_L SFG band undergoes a redshift with electrode potential increasing due to the electrochemical Stark effect. The Stark slope between -0.3 and -1.1 V is 26.8 $\text{cm}^{-1} \text{V}^{-1}$, smaller than that of the CO_2 reduction experiments because of the difference in electrode environments and CO coverage. Therefore, the 2100 cm^{-1} SFG band in the CO_2 reduction is the linearly bonded CO on the Au surface.

The BB-SFG spectra were dominated by the baseline fluctuations after the nonresonant normalization throughout the whole potential window even for the CO bubbled Cu electrodes, as shown in Fig. S7 (ESI[†]). There are several possible reasons for the absence of the C–O SFG band on Cu: (1) there is no or too little linearly bonded CO to be detected; (2) surface $\ast\text{CO}$ undergoes fast reactions and converts into other species in a very short time; (3) the surface CO is adsorbed in such a manner that is unfavourable for SFG measurement since SFG is sensitive to the surface arrangement, such as orientation, packing, and adsorption sites.^{72,73} The theoretical and experimental findings suggest that CO can adsorb on the Cu surface. From the DFT simulation, the binding energy of CO–Cu is greater than that of CO–Au.^{29,74} Hori *et al.* found that CO was reversibly adsorbed in an on-top manner on (1 0 0) or (1 1 1) step sites, but not on the (1 1 1) terrace sites of Cu in their IR spectroscopy study of single crystal Cu electrodes.^{32,38,47} Wuttig *et al.* also observed CO_L on a Cu film using ATR-SEIRAS and probed the variation in CO surface population during CO_2 reduction.⁴⁸ Zhu *et al.* detected CO_L on Cu in both CO_2 -saturated and Ar-saturated KHCO_3 solutions.⁴⁹ In our *in situ* FTIRS experiments (details in the ESI[†]), a band near 2055 cm^{-1} was detected and assigned to CO_L , and no other bands could be assigned to CO on the Cu film electrode. We believe that in our case, CO is adsorbed on the Cu surface, but not in an ordered on-top manner as on the Au surface. Subsequently, surface $\ast\text{CO}$ converted to other structures under

the reduction condition. Koper *et al.* reported that a hydrogenated CO dimer intermediate (OCCOH) can be detected with FTIR at low overpotentials in LiOH solutions on Cu(100), followed by the formation of other C_2 species.⁶ The difference in the surface arrangements could be the reason for the formation of the C–C bond on Cu but not on Au surfaces. Our SFG results could be helpful for the understanding of the mechanism of CO_2 reduction on Cu, and will be an efficient complement to other *in situ* spectroscopic studies.

BB-SFG spectra in the C–H stretching spectral range

Besides the surface CO species, there are many hydrocarbon intermediates and products of the CO_2 reduction on Cu electrodes. It is important to directly observe any possible C–H vibrations to better understand the reaction pathways and mechanisms. Fig. 6(a) displays the BB-SFG spectra during electrochemical CO_2 reduction with the IR tuned to 3400 nm covering 2850 – 3050 cm^{-1} . At -0.6 V, no resonant SFG features were observed. Around -0.8 V, new spectral features, two resonant SFG bands, appeared, and the intensity of the two narrow SFG bands gradually varied with electrode potential and nearly disappeared at -1.5 V.

To better analyse the evolution of the SFG spectra, eqn (3) was adopted to fit the BB-SFG spectra, and the results are displayed in Fig. 6(b–d). Two resonant BB-SFG bands around 2936 cm^{-1} (band 1) and 2996 cm^{-1} (band 2) could be clearly observed with almost fixed positions during the reaction, while their intensities gradually reached the maximum at -1.1 V, as shown in Fig. 6(d). The two resonant BB-SFG bands evolved with electrode potential identically, implying that these BB-SFG bands correspond to the same hydrocarbon intermediate of the

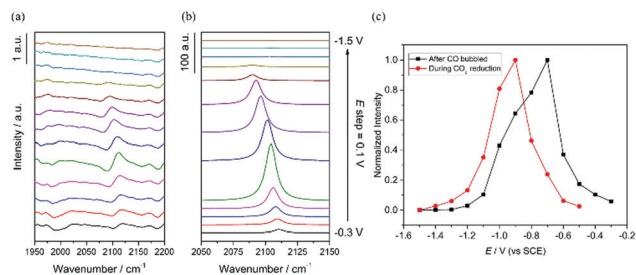


Fig. 5 Potential-dependent BB-SFG spectra (a) and fitting results (b) for CO adsorbed on Au electrode in 0.1 M NaClO_4 solution (normalized with the broadband nonresonant). Offset for comparison. (c) Potential-dependent SFG band intensity of CO_L (black for bubbled CO on Au, and red for CO_2 reduction on Au). Offset for comparison.

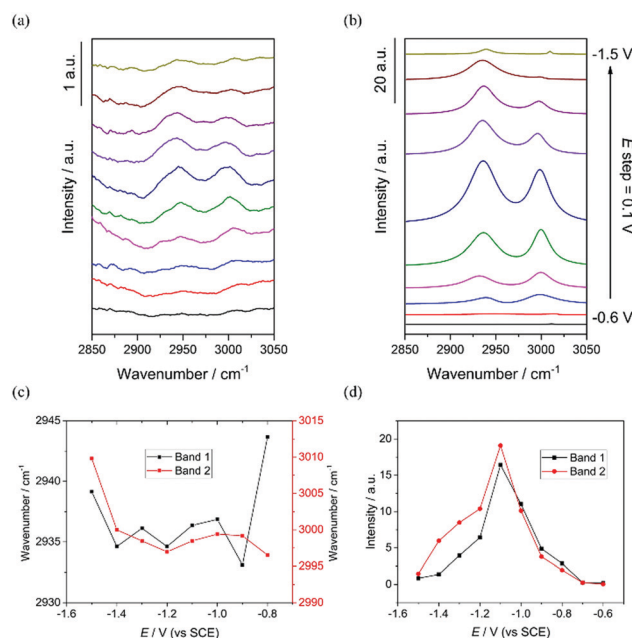


Fig. 6 Potential-dependent BB-SFG spectra (C–H region) (a) and fitting data (b) of CO_2 reduction in 0.1 M CO_2 -saturated NaHCO_3 solution at Cu electrode (normalized with the broadband nonresonant). Offset for comparison. Variations of resonant band position (c) and intensity (d).

CO₂ reduction process. The band at 2996 cm⁻¹ is higher than that of the typical C–H stretching vibrations of any alkanes. It is most likely from hydrocarbons with strong electron-withdrawing groups, such as aldehydes and alcohols (or alkoxy), and blueshifted due to the interactions with Cu. Fig. 7(a) displays one possible ethylene/ethanol pathway of CO₂ reduction on a Cu surface proposed by Koper *et al.*, which may relate to this work.^{4,7,25} We can rule out those intermediates with only one H atom (only one possible C–H vibration) and those with only H bonded to the C–C double bond (C–H stretching at more than 3000 cm⁻¹). The Cu-ethoxy intermediate and its previous step both consist of 2 C–H groups. If the 2 observed SFG bands both come from the methyl group, then the 2996 cm⁻¹ band should be the asymmetric C–H stretching and the band at 2936 cm⁻¹ corresponds to the Fermi resonance (symmetric stretching at a much lower frequency), both blueshifted due to the interaction with Cu. However, regular asymmetric stretching and Fermi resonance of the methyl group of ethanol locate at 2970 cm⁻¹ and 2926 cm⁻¹,^{75,76} if both are blueshifted by the same amount (though the same mechanism), then the band at 2936 cm⁻¹ is relatively too low. Additionally, the CH₃–CH₂–O–Cu intermediate is more stable than CH₃–CH–O–Cu. Therefore, we assign the 2996 cm⁻¹ and 2936 cm⁻¹ BB-SFG bands to the asymmetric C–H stretching of the methyl and methylene groups of the surface ethoxy group, respectively. The missing of the symmetric C–H stretching BB-SFG bands is due to the orientation of the ethoxy group on the Cu surface that favoured the asymmetric vibrations. Under the *ppp* polarization combination in our BB-SFG measurement, only those vibrations with strong enough vertical components (perpendicular to the Cu surface) can contribute to the SFG signal significantly.^{72,77,78} Therefore, if the dipole of the symmetric C–H stretching of the ethoxy group oriented parallel or close to parallel to the Cu surface, then only the asymmetric vibrations can be observed in the BB-SFG spectra. The ethoxy group adsorbed at the Cu surface with a tilted angle from the surface normal, as shown in Fig. 7(b). Additionally, our SFG measurement of ethanol–water solution on the Au surface observed two SFG bands around 2930 and

2995 corresponding with the C–H stretching of the ethanol as well, as shown in Fig. S7 (ESI[†]). Therefore, the two SFG bands observed in this paper can be assigned to the asymmetric C–H stretching of the methyl and methylene groups of the surface Cu–ethoxy intermediate, which is the precursor of ethanol.

For comparison, the potential-dependent BB-SFG spectra of CO₂ reduction on the Au electrode and UPD-Cu/Au electrodes under the same conditions as that on Cu have been recorded and are shown in Fig. 8. No clear resonant SFG band was observed. The coverage area of UPD-Cu is relatively low (<5%, see Fig. S5 and Table S1 (ESI[†]) for details); thus, with such a low Cu coverage, it is hard to detect significant hydrocarbon products on UPD-Cu/Au as compared to that on the Cu electrode.

Overall, on the Cu surface, two C–H vibrations from the methyl and methylene groups were observed with an onset potential of about –0.7 V. The variations of the intensities of these two SFG bands were similar during potential scanning, indicating that the two bands originated from the same adsorbate, the relatively stable Cu-ethoxy intermediate, a reaction intermediate in the ethanol pathway. In the entire potential window, no *CO SFG band was found on Cu. This result indicates that the important intermediate *CO exists in disordered orientations on Cu, and the disordered adsorption manner may contribute to the C–C bond formation for the further conversion to C₂ products. Our findings are consistent with the proposed reaction pathways of CO₂ reduction on Cu by Koper *et al.*,^{4,7,25} and the stable intermediate Cu-ethoxy is directly observed by the *in situ* SFG technique. On the Au surface, CO_L was observed at an earlier onset potential of –0.5 V and no hydrocarbons were identified. The uniform linear adsorption of CO hinders the further reaction on Au. With the modification of the UPD Cu sub-monolayer on Au, the CO_L SFG band intensity decreased remarkably but the feature of intensity variation remained the same, which suggests that part of the Au reaction sites were hindered by UPD Cu. From these results, it can be concluded that the CO₂ reduction pathways on Cu and Au electrodes are obviously different. The uniform linear adsorption of CO hindered the further reaction on the Au surface.

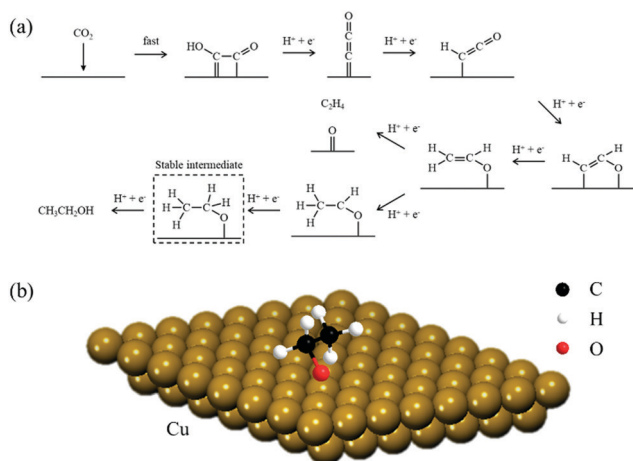


Fig. 7 (a) Mechanism for the C₂ pathway of CO₂ reduction on Cu. (b) Cu-ethoxy intermediate on Cu.

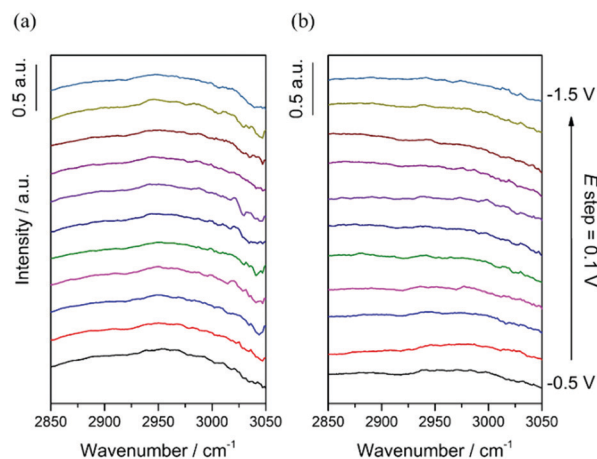


Fig. 8 Potential-dependent BB-SFG spectra (C–H region) of 0.1 M CO₂-saturated NaHCO₃ solution on (a) Au and (b) UPD-Cu/Au electrodes (normalized with the broadband nonresonant).

The disordered CO species on Cu made it possible for the formation of C2 intermediates.

Conclusions

In conclusion, by performing *in situ* electrochemical SFG spectroscopy, we have investigated the role of Cu and Au during CO₂ electrochemical reduction. On the Cu surface, we observed the ethoxy intermediate (Cu–OCH₂CH₃) at an electrode potential <–0.7 V and no obvious *CO in 0.1 M CO₂-saturated NaHCO₃ solution. While on the Au surface, linearly adsorbed CO could be detected. Therefore, under the present experimental conditions, CO may be disorderly adsorbed on Cu, which favors the formation of the C–C bond and C2 intermediates. However, a full roadmap of the CO₂ reduction cannot be drawn with the current findings. Future experiments in broader spectral ranges and simulations will be carried out to further analyze the mechanism of CO₂ reduction.

Conflicts of interest

There are no conflicts to declare.

Acknowledgements

The study was supported by NSFC (21327901, and 21621091) and the National Key Research and Development Program of China (2016YFA0200702, and 2017YFA0206500).

Notes and references

- 1 Y. Hori, in *Modern Aspects of Electrochemistry*, ed. C. G. Vayenas, R. E. White and M. E. Gamboa-Aldeco, Springer, New York, NY, 2008, DOI: 10.1007/978-0-387-49489-0_3, ch. 3, pp. 89–189.
- 2 M. Rakowski DuBois and D. L. DuBois, *Acc. Chem. Res.*, 2009, **42**, 1974–1982.
- 3 D. T. Whipple and P. J. A. Kenis, *J. Phys. Chem. Lett.*, 2010, **1**, 3451–3458.
- 4 F. Calle-Vallejo and M. T. Koper, *Angew. Chem., Int. Ed.*, 2013, **52**, 7282–7285.
- 5 M. C. Figueiredo, I. Ledezma-Yanez and M. T. M. Koper, *ACS Catal.*, 2016, **6**, 2382–2392.
- 6 E. Perez-Gallent, M. C. Figueiredo, F. Calle-Vallejo and M. T. Koper, *Angew. Chem., Int. Ed.*, 2017, **56**, 3621–3624.
- 7 R. Kortlever, J. Shen, K. J. Schouten, F. Calle-Vallejo and M. T. Koper, *J. Phys. Chem. Lett.*, 2015, **6**, 4073–4082.
- 8 H. Mistry, R. Reske, Z. Zeng, Z. J. Zhao, J. Greeley, P. Strasser and B. R. Cuenya, *J. Am. Chem. Soc.*, 2014, **136**, 16473–16476.
- 9 M. F. Baruch, J. E. Pander, J. L. White and A. B. Bocarsly, *ACS Catal.*, 2015, **5**, 3148–3156.
- 10 W. Zhu, Y. J. Zhang, H. Zhang, H. Lv, Q. Li, R. Michalsky, A. A. Peterson and S. Sun, *J. Am. Chem. Soc.*, 2014, **136**, 16132–16135.
- 11 R. Reske, H. Mistry, F. Beharfarid, B. Roldan Cuenya and P. Strasser, *J. Am. Chem. Soc.*, 2014, **136**, 6978–6986.
- 12 D. Gao, H. Zhou, J. Wang, S. Miao, F. Yang, G. Wang, J. Wang and X. Bao, *J. Am. Chem. Soc.*, 2015, **137**, 4288–4291.
- 13 X. Feng, K. Jiang, S. Fan and M. W. Kanan, *J. Am. Chem. Soc.*, 2015, **137**, 4606–4609.
- 14 W. Zhu, J. Ke, S. B. Wang, J. Ren, H. H. Wang, Z. Y. Zhou, R. Si, Y. W. Zhang and C. H. Yan, *ACS Catal.*, 2015, **5**, 1995–2008.
- 15 A. M. Ge, B. Rudshiteyn, B. T. Psciuk, D. Q. Xiao, J. Song, C. L. Anfuso, A. M. Ricks, V. S. Batista and T. Q. Lian, *J. Phys. Chem. C*, 2016, **120**, 20970–20977.
- 16 Y. Hori, H. Wakebe, T. Tsukamoto and O. Koga, *Electrochim. Acta*, 1994, **39**, 1833–1839.
- 17 M. Azuma, *J. Electrochem. Soc.*, 1990, **137**, 1772–1778.
- 18 C. Costentin, G. Passard, M. Robert and J. M. Saveant, *J. Am. Chem. Soc.*, 2014, **136**, 11821–11829.
- 19 A. S. Varela, N. Ranjbar Sahraie, J. Steinberg, W. Ju, H. S. Oh and P. Strasser, *Angew. Chem., Int. Ed.*, 2015, **54**, 10758–10762.
- 20 I. Azcarate, C. Costentin, M. Robert and J. M. Saveant, *J. Am. Chem. Soc.*, 2016, **138**, 16639–16644.
- 21 Y. Hori, K. Kikuchi and S. Suzuki, *Chem. Lett.*, 1985, 1695–1698.
- 22 S. Nitopi, E. Bertheussen, S. B. Scott, X. Liu, A. K. Engstfeld, S. Horch, B. Seger, I. E. L. Stephens, K. Chan, C. Hahn, J. K. Nørskov, T. F. Jaramillo and I. Chorkendorff, *Chem. Rev.*, 2019, **119**, 7610–7672.
- 23 A. A. Peterson, F. Abild-Pedersen, F. Studt, J. Rossmeisl and J. K. Nørskov, *Energy Environ. Sci.*, 2010, **3**, 1311–1315.
- 24 M. Gattrell, N. Gupta and A. Co, *Energy Convers. Manage.*, 2007, **48**, 1255–1265.
- 25 K. J. P. Schouten, Y. Kwon, C. J. M. van der Ham, Z. Qin and M. T. M. Koper, *Chem. Sci.*, 2011, **2**, 1902–1909.
- 26 X. Nie, M. R. Esopi, M. J. Janik and A. Asthagiri, *Angew. Chem., Int. Ed.*, 2013, **52**, 2459–2462.
- 27 Y. Hori, A. Murata and R. Takahashi, *J. Chem. Soc., Faraday Trans. 1*, 1989, **85**, 2309–2326.
- 28 Y. Hori, A. Murata, T. Tsukamoto, H. Wakebe, O. Koga and H. Yamazaki, *Electrochim. Acta*, 1994, **39**, 2495–2500.
- 29 K. P. Kuhl, E. R. Cave, D. N. Abram and T. F. Jaramillo, *Energy Environ. Sci.*, 2012, **5**, 7050–7059.
- 30 B. Jermann and J. Augustynski, *Electrochim. Acta*, 1994, **39**, 1891–1896.
- 31 G. Kyriacou and A. Anagnostopoulos, *J. Electroanal. Chem.*, 1992, **322**, 233–246.
- 32 Y. Hori, A. Murata and Y. Yoshinami, *J. Chem. Soc., Faraday Trans.*, 1991, **87**, 125–128.
- 33 Y. Hori, A. Murata, R. Takahashi and S. Suzuki, *J. Am. Chem. Soc.*, 1987, **109**, 5022–5023.
- 34 K. Watanabe, U. Nagashima and H. Hosoya, *Appl. Surf. Sci.*, 1994, **75**, 121–124.
- 35 D. W. Dewulf, T. Jin and A. J. Bard, *J. Electrochem. Soc.*, 1989, **136**, 1686–1691.
- 36 Y. Hori, R. Takahashi, Y. Yoshinami and A. Murata, *J. Phys. Chem. B*, 1997, **101**, 7075–7081.
- 37 K. Watanabe, U. Nagashima and H. Hosoya, *Chem. Phys. Lett.*, 1993, **209**, 109–110.
- 38 Y. Hori, H. Wakebe, T. Tsukamoto and O. Koga, *Surf. Sci.*, 1995, **335**, 258–263.

- 39 Y. Zheng, A. Vasileff, X. Zhou, Y. Jiao, M. Jaroniec and S. Z. Qiao, *J. Am. Chem. Soc.*, 2019, **141**, 7646–7659.
- 40 A. J. Garza, A. T. Bell and M. Head-Gordon, *ACS Catal.*, 2018, **8**, 1490–1499.
- 41 H. Xiao, T. Cheng and W. A. Goddard, 3rd, *J. Am. Chem. Soc.*, 2017, **139**, 130–136.
- 42 M. Dunwell, Y. S. Yan and B. J. Xu, *ACS Catal.*, 2017, **7**, 5410–5419.
- 43 J. E. Pander, M. F. Baruch and A. B. Bocarsly, *ACS Catal.*, 2016, **6**, 7824–7833.
- 44 J. Heyes, M. Dunwell and B. Xu, *J. Phys. Chem. C*, 2016, **120**, 17334–17341.
- 45 C. M. Gunathunge, X. Li, J. Y. Li, R. P. Hicks, V. J. Ovalle and M. M. Waegle, *J. Phys. Chem. C*, 2017, **121**, 12337–12344.
- 46 L. Wang, K. Gupta, J. B. M. Goodall, J. A. Darr and K. B. Holt, *Faraday Discuss.*, 2017, **197**, 517–532.
- 47 O. Koga, S. Teruya, K. Matsuda, M. Minami, N. Hoshi and Y. Hori, *Electrochim. Acta*, 2005, **50**, 2475–2485.
- 48 A. Wuttig, C. Liu, Q. Peng, M. Yaguchi, C. H. Hendon, K. Motobayashi, S. Ye, M. Osawa and Y. Surendranath, *ACS Cent. Sci.*, 2016, **2**, 522–528.
- 49 S. Zhu, B. Jiang, W.-B. Cai and M. Shao, *J. Am. Chem. Soc.*, 2017, **139**, 15664–15667.
- 50 B. A. Rosen, J. L. Haan, P. Mukherjee, B. Braunschweig, W. Zhu, A. Salehi-Khojin, D. D. Dlott and R. I. Masel, *J. Phys. Chem. C*, 2012, **116**, 15307–15312.
- 51 N. García Rey and D. D. Dlott, *J. Phys. Chem. C*, 2015, **119**, 20892–20899.
- 52 B. Braunschweig, P. Mukherjee, J. L. Haan and D. D. Dlott, *J. Electroanal. Chem.*, 2017, **800**, 144–150.
- 53 A. Ge, B. Rudshiteyn, P. E. Videla, C. J. Miller, C. P. Kubiak, V. S. Batista and T. Lian, *Acc. Chem. Res.*, 2019, **52**, 1289–1300.
- 54 A. M. Ge, P. E. Videla, B. Rudshiteyn, Q. L. Liu, V. S. Batista and T. Q. Lian, *J. Phys. Chem. C*, 2018, **122**, 13944–13952.
- 55 A. Ge, B. Rudshiteyn, J. Zhu, R. J. Maurer, V. S. Batista and T. Lian, *J. Phys. Chem. Lett.*, 2018, **9**, 406–412.
- 56 M. L. Clark, A. Ge, P. E. Videla, B. Rudshiteyn, C. J. Miller, J. Song, V. S. Batista, T. Lian and C. P. Kubiak, *J. Am. Chem. Soc.*, 2018, **140**, 17643–17655.
- 57 J. J. Wang, M. Xu, Z. C. Huangfu, Y. Wang, Y. H. He, W. Guo and Z. H. Wang, *Vib. Spectrosc.*, 2016, **85**, 122–127.
- 58 Q. Cen, Y. He, M. Xu, J. Wang and Z. Wang, *J. Chem. Phys.*, 2015, **142**, 114201.
- 59 Y. H. He, G. Q. Chen, M. Xu, Y. Q. Liu and Z. H. Wang, *J. Lumin.*, 2014, **152**, 244–246.
- 60 X. D. Zhu, H. Suhr and Y. R. Shen, *Phys. Rev. B: Condens. Matter Mater. Phys.*, 1987, **35**, 3047–3050.
- 61 Y. R. Shen, *Nature*, 1989, **337**, 519–525.
- 62 Y. R. Shen, *Annu. Rev. Phys. Chem.*, 1989, **40**, 327–350.
- 63 Y. R. Shen, *Appl. Phys. A: Mater. Sci. Process.*, 1994, **59**, 541–543.
- 64 Y. R. Shen, *Surf. Sci.*, 1994, **299**, 551–562.
- 65 Y. R. Shen, *J. Phys. Chem. C*, 2012, **116**, 15505–15509.
- 66 S. G. Sun, W. B. Cai, L. J. Wan and M. Osawa, *J. Phys. Chem. B*, 1999, **103**, 2460–2466.
- 67 M. H. Shao and R. R. Adzic, *J. Phys. Chem. B*, 2005, **109**, 16563–16566.
- 68 M. Ma, Y. G. Yan, S. J. Huo, Q. J. Xu and W. B. Cai, *J. Phys. Chem. B*, 2006, **110**, 14911–14915.
- 69 S. C. Chang, A. Hamelin and M. J. Weaver, *Surf. Sci.*, 1990, **239**, L543–L547.
- 70 S. C. Chang and M. J. Weaver, *J. Phys. Chem.*, 1991, **95**, 5391–5400.
- 71 H. Miyake, S. Ye and M. Osawa, *Electrochem. Commun.*, 2002, **4**, 973–977.
- 72 X. Zhuang, P. B. Miranda, D. Kim and Y. R. Shen, *Phys. Rev. B: Condens. Matter Mater. Phys.*, 1999, **59**, 12632–12640.
- 73 F. C. B. Maia and P. B. Miranda, *J. Phys. Chem. C*, 2015, **119**, 7386–7399.
- 74 T. Jiang, D. J. Mowbray, S. Dobrin, H. Falsig, B. Hvolbaek, T. Bligaard and J. K. Nørskov, *J. Phys. Chem. C*, 2009, **113**, 10548–10553.
- 75 R. Lu, W. Gan, B.-H. Wu, H. Chen and H.-F. Wang, *J. Phys. Chem. B*, 2004, **108**, 7297–7306.
- 76 R. Lu, W. Gan, B. H. Wu, Z. Zhang, Y. Guo and H. F. Wang, *J. Phys. Chem. B*, 2005, **109**, 14118–14129.
- 77 M. B. Feller, W. Chen and Y. R. Shen, *Phys. Rev. A: At., Mol., Opt. Phys.*, 1991, **43**, 6778–6792.
- 78 A. G. Lambert, P. B. Davies and D. J. Neivandt, *Appl. Spectrosc. Rev.*, 2005, **40**, 103–145.